Analysis of heat and mass transfer in a countercurrent-flow wet surface heat exchanger

Y. L. Tsay
Department of Power Mechanical Engineering, National Yuenlin Polytechnic Institute, Huwei, Yuenlin, Taiwan, ROC

A numerical analysis was carried out to study the detailed heat- and mass-transfer characteristics in a countercurrent-flow wet surface heat exchanger. The coupled conservation equations for hot fluid, liquid film and moist air stream are solved together. The heat-transfer rates in the wet surface heat exchanger are compared with those obtainable in the dry surface heat exchanger. Furthermore great attention is paid to investigating the effects of latent heat transfer associated with liquid-film vaporization on the thermal performance of the exchanger. Results show that the energy transported across the liquid film is mostly absorbed by the process of film vaporization.

Keywords: heat and mass transfer; wet surface heat exchanger; latent heat transfer

Introduction

Wet surface heat exchangers are widely used in refrigerating, air conditioning and powerplant systems. In these heat exchangers, both air and liquid water are used as the cooling media. The hot fluid stream on one side of the heat-transfer surface rejects heat to the falling liquid water film and moist air stream on the other side. Because a part of liquid water evaporates into the air stream, latent and sensible heat transfer occurs at the liquid film-air interface simultaneously. The latent heat transport in connection with the vaporization of liquid film plays an important role in the transfer processes and greatly enhances the heat transfer over that obtainable in a dry surface heat exchanger (see, e.g., El-Wakil 1984; Tsay et al. 1990). Furthermore, the wet-bulb temperature of the air stream can strongly influence the evaporation rate of the liquid film. Thus, if properly designed, the temperature of the hot fluid stream in a wet surface heat exchanger can be cooled to a degree considerably lower than that in a dry surface heat exchanger and thus improves thermal efficiency of power or refrigerating cycles (Guinn and Novel 1981; Holzhauer 1979; Kafesgian et al. 1961; Leidenfrost and Korenic 1979).

Mizushima et al. (1967) experimentally studied the performance of horizontal-tube evaporative coolers. The influences of the Reynolds numbers of the cooling water and of the air flow on the heat- and mass-transfer coefficients were presented. The effects of spraying a mist of water on air stream flowing through a compact tube-and-fin–type heat exchanger were investigated by Jang and Clark (1975). Great enhancements in heat-transfer performance were reported. The heat and mass transfer in a vertical-tube evaporative cooler was experimentally examined by Perez-Blanco and Bird (1984). Their results show that the controlling resistance to heat and mass transfer in the evaporative cooler occurs at the liquid-air interface.

The analysis of the transfer processes in a wet surface heat exchanger are inherently complex owing to the many conservation equations to be solved, and the nonlinear coupling of momentum, heat and mass transfer at the liquid film-air interface. Thus a one-dimensional (1-D) model has been used in previous theoretical studies to determine the performance of a wet surface heat exchanger. Maclaine-Cross and Banks (1972, 1981) have analyzed the heat- and mass-transfer characteristics in a wet surface heat exchanger. A linear approximation to the saturation line was proposed by them to simplify the conservation equations. In addition, the Lewis relation was assumed to be satisfied and the surface of the water film was considered at the same temperature. Their predicted performance of the heat exchanger is substantially higher than that measured by Pescod (1979). A similar 1-D analytic method was also used by Kettleborough and Hsieh (1983) to study the wet surface plastic heat exchanger. It was reported that the wet-bulb temperature of the refrigerant moist air stream is an important factor affecting the effectiveness of the exchanger. Wassel and Mills (1987) illustrated a design methodology for a countercurrent falling film evaporative cooler. The narrow flow passages were found to be more effective for the evaporative condenser.

The preceding review reveals that the detailed interactions between the hot fluid and cooling media were not properly treated in the literature. The purpose of this study is to enhance the understanding of the heat- and mass-transfer processes in a countercurrent-flow multichannel wet surface heat exchanger by performing a detailed numerical analysis. Thus, a conjugate heat- and mass-transfer problem is considered here to examine the interactions between the hot and cold flow streams along with the liquid film vaporization. Shown in Figure 1 is the schematic diagram of a representative unit of flow passages in the multichannel heat exchanger to be investigated. The countercurrent fluid on the hot side enters the vertical channel with a uniform inlet velocity $u_{h,in}$ and temperature $T_{h,in}$.

Address reprint requests to Dr. Tsay at the Department of Power Mechanical Engineering, National Yuenlin Polytechnic Institute, Huwei, Yuenlin, 63208, Taiwan, ROC.

Received 21 February 1993; accepted 27 September 1993

Meanwhile the moist air stream flows over a liquid water film on the cold side with the uniform inlet velocity $u_{c,in}$, temperature $T_{c,in}$ and water vapor concentration w_{in}. The right-side surface of the plate is uniformly wetted by a thin liquid film with a uniform inlet temperature $T_{h,in}$ and film thickness $\delta_{l,in}$. The hot fluid rejects heat through the plate to the liquid film and moist air stream. As the liquid film falls down along the plate, a part of liquid water evaporates into the air stream. Thus, both the sensible and latent heat transfer occur at the film-air interface. The coupled conservation equations for hot fluid, liquid film and moist air stream are solved together. The matching conditions at the liquid–moist air interface are rigorously treated. Attention is paid to examining the effects of latent heat transport on the performance of the wet surface heat exchanger and the differences in heat-transfer rates in the wet and dry surface heat exchangers.

Analysis

In an initial effort to study the effects of liquid-film vaporization on the heat exchange between the hot and cold fluids in wet surface heat exchangers, the wave motion of the film-air interface and the entrainment of the liquid in the form of droplets into the moist-air stream are neglected in the present study because of the lack of adequate information for these rather complicated processes.

Basic equations for liquid film

Because only thin liquid film is considered here, the inertial terms in the momentum equation are small compared with the body force term and hence can be neglected (Shembharkar and Pai 1986; Stücheli and Özisik 1976). Furthermore, for a thin liquid film the longitudinal gradients of velocity and temperature are much smaller than those in the transverse direction. With these simplifications the steady laminar momentum and heat transfer in the liquid film can be described by the following equations:

x Momentum equation:

$$\nu_l \frac{\partial^2 u_l}{\partial y^2} + g - \frac{1}{\rho_l}\frac{dp_c}{dx} = 0 \tag{1}$$

Energy equation:

$$u_l \frac{\partial T_l}{\partial x} = \alpha_l \frac{\partial^2 T_l}{\partial y^2} \tag{2}$$

Notation

b	channel width
D	mass diffusivity
E_m	dimensionless evaporation rate of liquid film, Equation 30
g	gravitational acceleration
h_{fg}	latent heat of vaporization
h_m	local mass-transfer coefficient
h_t	local heat-transfer coefficient
k	thermal conductivity
l	channel length
L	dimensionless channel length, l/b
M	molecular weight
$\dot{m}_l$	mass-flow rate of liquid film per unit channel depth
$m''_{v,i}$	evaporating mass flux of water vapor at interface
Nu	Nusselt number
p	pressure
P_h	dimensionless parameter, $[(p_h - \rho_h g x) - p_{h,in}]/(\rho_h u^2_{h,in})$
P_c	dimensionless parameter, $[(p_c - \rho_c g x) - p_{c,in}]/(\rho_c u^2_{c,in})$
Pr	Prandtl number, ν/α
q''	heat flux
Q''_w	dimensionless wall heat flux
Re_h	Reynolds number of hot fluid, $2u_{h,in}b/\nu_h$
$Re_{c,in}$	Reynolds number of moist air at inlet, $2u_{c,in}b/\nu_c$
$Re_{l,in}$	Reynolds number of liquid film at inlet, $4\dot{m}_{l,in}/\mu_l$
S	Parameter, $[\rho_c D h_{fg}(w_r - w_{in})]/[k_c(T_{h,in} - T_{c,in})]$
Sc	Sherwood number, ν_c/D
T	temperature
u	longitudinal velocity
U_c	dimensionless longitudinal velocity of moist air, $u_c/u_{c,in}$
U_h	dimensionless longitudinal velocity of hot fluid, $u_h/u_{h,in}$
U_l	dimensionless longitudinal velocity of liquid film, $u_l/u_{l,in}$
v	transverse velocity
V_c	dimensionless transverse velocity of moist air, $2lv_c/(\nu_c Re_{c,in})$
V_h	dimensionless transverse velocity of hot fluid, $2lv_h/(\nu_h Re_h)$
w	mass fraction of water vapor
w_r	saturated mass fraction of water vapor at inlet temperature of hot fluid
W	dimensionless mass fraction of water vapor, $(w - w_{in})/(w_r - w_{in})$
x	longitudinal coordinate
X	dimensionless longitudinal coordinate, x/l
y	transverse coordinate
Y	dimensionless transverse coordinate, y/b

Greek letters

α	thermal diffusivity
θ	dimensionless temperature, $(T - T_{c,in})/(T_{h,in} - T_{c,in})$
μ	dynamic viscosity
ν	kinematic viscosity
ρ	density
δ	thickness of liquid film
ϕ	relative humidity of moist air

Subscripts

a	air
b	bulk quantity
c	moist air
e	latent heat
h	hot fluid
i	liquid film-air interface
in	inlet
l	liquid film
s	sensible heat
v	vapor

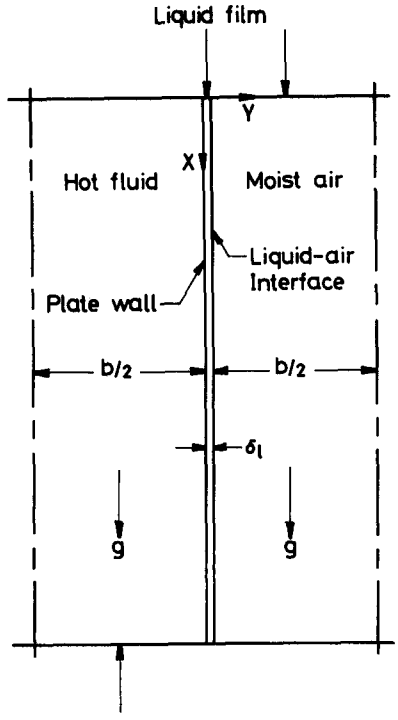

Figure 1 Schematic diagram of the physical system

Basic equations for hot fluid

By adopting the boundary layer approximation, the steady laminar convection flow of hot fluid in a vertical channel can be described by the basic equations as follows:

Continuity equation:

$$\frac{\partial u_h}{\partial x} + \frac{\partial v_h}{\partial y} = 0 \tag{3}$$

x Momentum equation:

$$u_h \frac{\partial u_h}{\partial x} + v_h \frac{\partial u_h}{\partial y} = -\frac{1}{\rho_h}\frac{dp_h}{dx} + \nu_h \frac{\partial^2 u_h}{\partial y^2} + g \tag{4}$$

Energy equation:

$$u_h \frac{\partial T_h}{\partial x} + v_h \frac{\partial T_h}{\partial y} = \alpha_h \frac{\partial^2 T_h}{\partial y^2} \tag{5}$$

Basic equations for moist air stream

Continuity equation:

$$\frac{\partial u_c}{\partial x} + \frac{\partial v_c}{\partial y} = 0 \tag{6}$$

x Momentum equation:

$$u_c \frac{\partial u_c}{\partial x} + v_c \frac{\partial u_c}{\partial y} = -\frac{1}{\rho_c}\frac{dp_c}{dx} + \nu_h \frac{\partial^2 u_c}{\partial y^2} + g \tag{7}$$

Energy equation:

$$u_c \frac{\partial T_c}{\partial x} + v_c \frac{\partial T_c}{\partial y} = \alpha_c \frac{\partial^2 T_c}{\partial y^2} \tag{8}$$

Equation of species diffusion for water vapor:

$$u_c \frac{\partial w}{\partial x} + v_c \frac{\partial w}{\partial y} = D \frac{\partial^2 w}{\partial y^2} \tag{9}$$

Interface matching conditions

In the present study the matching conditions for the liquid film and air stream at the film-air interface, $y = \delta_l$, are carefully treated as follows:

1. Continuity of velocity, temperature and shear stress

$$u_{l,i} = u_{c,i},\ T_{l,i} = T_{c,i},\ \left(\mu_l \frac{\partial u_l}{\partial y}\right)_i = \left(\mu_c \frac{\partial u_c}{\partial y}\right)_i \tag{10}$$

2. Notice that the interface is semi-permeable, that is, the solubility of air in liquid water is negligibly small, and the air is stationary at the interface. The transverse velocity of the air-water vapor mixture can be computed by the equation

$$v_{c,i} = -\left(\frac{D}{1-w}\frac{\partial w}{\partial y}\right)_i \tag{11}$$

3. Assuming the interface to be at thermodynamic equilibrium and the air-water vapor mixture as an ideal gas mixture, the mass fraction of the water vapor is calculated by (Eckert and Drake 1972)

$$w_i = \frac{M_v p_{v,i}}{M_a(p_c - p_{v,i}) + M_v p_{v,i}} \tag{12}$$

where $p_{v,i}$ is the saturation pressure of water vapor at the interface temperature.

4. Energy balance at the interface

$$-\left(k_l \frac{\partial T_l}{\partial y}\right)_i = -\left(k_c \frac{\partial T_c}{\partial y}\right)_i + m''_{v,i} h_{fg} \tag{13}$$

where the evaporating flux of water vapor $m''_{v,i}$ is evaluated by

$$m''_{v,i} = -\left(\frac{\rho_c D}{1-w}\frac{\partial w}{\partial y}\right)_i \tag{14}$$

In terms of the nondimensional variables the governing equations are as follows:

Hot fluid:

$$\frac{\partial U_h}{\partial X} + \frac{\partial V_h}{\partial Y} = 0 \tag{15}$$

$$U_h \frac{\partial U_h}{\partial X} + V_h \frac{\partial U_h}{\partial Y} = -\frac{dP_h}{dX} + \frac{2L}{\mathrm{Re}_h}\frac{\partial^2 U_h}{\partial Y^2} \tag{16}$$

$$U_h \frac{\partial \theta_h}{\partial X} + V_h \frac{\partial \theta_h}{\partial Y} = \frac{2L}{\mathrm{Pr}_h \mathrm{Re}_h}\frac{\partial^2 \theta_h}{\partial Y^2} \tag{17}$$

Moist air stream:

$$\frac{\partial U_c}{\partial X} + \frac{\partial V_c}{\partial Y} = 0 \tag{18}$$

$$U_c \frac{\partial U_c}{\partial X} + V_c \frac{\partial U_c}{\partial Y} = -\frac{dP_c}{dX} + \frac{2L}{\mathrm{Re}_{c,in}}\frac{\partial^2 U_c}{\partial Y^2} \tag{19}$$

$$U_c \frac{\partial \theta_c}{\partial X} + V_c \frac{\partial \theta_c}{\partial Y} = \frac{2L}{\mathrm{Pr}_c \mathrm{Re}_{c,in}}\frac{\partial^2 \theta_c}{\partial Y^2} \tag{20}$$

$$U_c \frac{\partial W}{\partial X} + V_c \frac{\partial W}{\partial Y} = \frac{2L}{\mathrm{Sc}\mathrm{Re}_{c,in}}\frac{\partial^2 W}{\partial Y^2} \tag{21}$$

Liquid film:

$$\frac{\partial^2 U_l}{\partial Y^2} - \left(\frac{\mathrm{Re}_{l,in}}{2L}\right)\left(\frac{b/2}{\delta_{l,in}}\right)\left[\left(\frac{\rho_c u_{c,in}^2}{\rho_l u_{l,in}^2}\right)\left(\frac{dP_c}{dX}\right) + \frac{(\rho_c - \rho_l)gl}{\rho_l U_{l,in}^2}\right] = 0 \quad (22)$$

$$\left(\frac{b/2}{\delta_{l,in}}\right) U_l \frac{\partial \theta_l}{\partial X} = \frac{2L}{\mathrm{Pr}_l \mathrm{Re}_{l,in}} \frac{\partial^2 \theta_l}{\partial Y^2} \quad (23)$$

The preceding equations are subjected to the following boundary and interface matching conditions:

$$\text{at } X = 0,\ U_c = 1,\ \theta_c = W = 0,\ \theta_l = \theta_{l,in} \quad (24a)$$

$$\text{at } X = 1,\ U_h = \theta_h = 1$$

$$\text{at } Y = -\frac{1}{2},\ \frac{\partial U_h}{\partial Y} = \frac{\partial \theta_h}{\partial Y} = 0 \quad (24b)$$

$$\text{at } Y = 0,\ U_h = V_h = U_l = 0,\ \theta_h = \theta_l,\ \frac{\partial \theta_h}{\partial Y} = \left(\frac{k_l}{k_h}\right)\frac{\partial \theta_l}{\partial Y} \quad (24c)$$

$$\text{at } Y = \frac{1}{2},\ \frac{\partial U_c}{\partial Y} = \frac{\partial \theta_c}{\partial Y} = \frac{\partial W}{\partial Y} = 0 \quad (24d)$$

$$\text{at } Y = \frac{\delta_l}{b},\ U_l = \left(\frac{u_{c,in}}{u_{l,in}}\right)U_c,\ \theta_{l,i} = \theta_{c,i}$$

$$W_i = \frac{w_i - w_{in}}{w_r - w_{in}},\ V_{c,i} = -\frac{2L}{\mathrm{Re}_{c,in}}\left(\frac{w_r - w_{in}}{1 - w_i}\right)\frac{1}{\mathrm{Sc}}\left(\frac{\partial^2 W}{\partial Y}\right)_i \quad (24e)$$

$$\left(\frac{\partial U_c}{\partial Y}\right)_i = \left(\frac{\mu_l}{\mu_c}\right)^2\left(\frac{\rho_c}{\rho_l}\right)\left(\frac{\mathrm{Re}_{l,in}}{\mathrm{Re}_{c,in}}\right)\left(\frac{b/2}{\delta_{l,in}}\right)\left(\frac{\partial U_l}{\partial Y}\right)_i$$

$$\left(\frac{\partial \theta_l}{\partial Y}\right)_i = \left(\frac{k_c}{k_l}\right)\left(\frac{\partial \theta_c}{\partial Y}\right)_i + \frac{\rho_c D h_{fg}(w_r - w_{in})}{k_l(T_{h,in} - T_{c,in})(1 - w_i)}\left(\frac{\partial W}{\partial Y}\right)_i$$

The preceding thermal boundary conditions at the channel wall, $Y = 0$, assume the wall extremely thin and its thermal resistance can be ignored. In addition, because only low Reynolds number of liquid film is considered in the present study, the inlet film thickness, $\delta_{l,in}$, can be evaluated by (Bird et al. 1960)

$$\delta_{l,in} = \left(\frac{3\nu_l^2}{4g}\mathrm{Re}_{l,in}\right)^{1/3} \quad (25)$$

One constraint to be satisfied in the solution of a steady channel flow is the overall mass balance at every axial location.

Hot fluid:

$$\int_{-1/2}^{0} U_h dY = \frac{1}{2} \quad (26)$$

Moist air stream:

$$\int_{\delta_l/b}^{1/2} U_c dY - \int_0^X V_{c,i}\, dX = 1/2 - \left(\frac{\delta_{l,in}}{b}\right) \quad (27)$$

The preceding equations are used in the solution procedures to determine the $(-dP_h/dX)$ and $(-dP_c/dX)$ in the hot flow and moist air stream, respectively.

Solution method

Because the flows governed by Equations 15–23 are parabolic in X, the finite-difference solutions for these equations can be marched in the downstream direction. A fully implicit numerical scheme, in which the axial convection is approximated by the upstream difference and the transverse convection and diffusion terms by the central difference, is employed to transform the governing equations into finite-difference equations. Each system of finite-difference equations forms a tridiagonal matrix equation that can be efficiently solved by using the Thomas algorithm. For a given flow and thermal condition, a brief outline of the solution procedures is described as follows:

1. Assume a dimensionless temperature distribution along the plate wall.
2. For any longitudinal location, guess a dimensionless liquid film thickness δ_l/b and a dimensionless pressure gradient for moist air stream $(-dP_c/dX)$.
3. Solve Equations 18–23 for V_c, U_c, θ_c, W, U_l and θ_l.
4. Check if the relative error between two consecutive interactions $n-1$ and n is small enough, that is, $|C^n - C^{n-1}|/|C^n|_{max} < 10^{-4}$ for all nodal points where C represents the variables U_c, V_c, θ_c, W, U_l and θ_l. If not, repeat procedures 3 and 4.
5. Check the satisfaction of the overall mass balance for moist air stream (Equation 27). If not, guess a new $(-dP_c/dX)$ by Newton's method and repeat procedures 3–5.
6. Check the overall mass balance for liquid film by examining the satisfaction of the inequality.

$$\left|\frac{\frac{\delta_{l,in}}{b} - \left[\int_0^{\delta_l/b} U_l dY + \left(\frac{\mathrm{Re}_{c,in}}{\mathrm{Re}_{l,in}}\right)\left(\frac{\mu_c}{\mu_l}\right)\left(\frac{\delta_{l,in}}{b/2}\right)\int_0^X V_{c,i} dX\right]}{\left(\frac{\mathrm{Re}_{c,in}}{\mathrm{Re}_{l,in}}\right)\left(\frac{\mu_c}{\mu_l}\right)\left(\frac{\delta_{l,in}}{b/2}\right)\int_0^X V_{c,i} dX}\right| < 10^{-4} \quad (28)$$

   If Equation 28 is not satisfied, repeat procedures 2–6.
7. Apply the procedures 2–7, successively, to march the solutions of momentum, energy and water-vapor species diffusion equations for the cold fluid streams (liquid film and moist air) from $X = 0$ to $X = 1$.
8. The procedures employed to obtain the velocity and temperature fields of hot fluid stream are similar to those procedures 2–5. But the proceeding direction is $X = 1$ to $X = 0$.
9. Check the continuity of heat flux at the plate wall by examining the satisfaction of the inequality,

$$\max\left|\frac{(\partial\theta_h/\partial Y)_{Y=0} - (k_l/k_h)(\partial\theta_l/\partial Y)_{Y=0}}{(\partial\theta_h/\partial Y)_{Y=0}}\right| < 10^{-4} \quad (29)$$

   If equation 29 is satisfied, the solutions converge. Otherwise assume a new wall temperature distribution and repeat procedures 2–9. For all cases studied, about 120–150 iterations are necessary for convergence of the temperature distribution along the plate wall.

To account for the change in liquid-film thickness in the flow direction owing to the film vaporization, the finite-difference computational grid used must comply with the variations of computation domains with X. This was accomplished by first locating the interface at a given X-location, and then dividing the film and air regions in the Y-direction into n_l and n_c points, respectively. Thus the interface position was rigorously traced. This adjustment of grid in Y-direction necessitates numerical interpolation when evaluating the convection terms.

During the program test several grid sizes were employed. A comparison of the results for the distributions of $\theta_{b,h}$, $\theta_{b,l}$ and $\theta_{b,c}$, from these computations for a typical case is shown in Table 1. It is noted that the differences in the results obtained by using the 61 × 136 and 81 × 181 grids are always less

Table 1 Comparison of the dimensionless bulk temperature for various grid arrangements for case with $Re_h = 1{,}000$, $Re_{l,in} = 200$, $Re_{c,in} = 1{,}000$, $T_{h,in} = 60°C$, $T_{l,in} = T_{c,in} = 30°C$ and $\phi_{in} = 50$ percent

		51 × 91		61 × 136		81 × 181	
	X	$n_x=51$ $n_l=11$	$n_h=40$ $n_c=40$	$n_x=61$ $n_l=16$	$n_h=60$ $n_c=60$	$n_x=81$ $n_l=21$	$n_h=80$ $n_c=80$
$\theta_{b,h}$	0.1	0.7623		0.7671		0.7696	
	0.3	0.8501		0.8545		0.8571	
	0.6	0.9292		0.9331		0.9348	
	0.9	0.9738		0.9775		0.9789	
$\theta_{b,l}$	0.1	0.2411		0.2386		0.2371	
	0.3	0.5308		0.5274		0.5257	
	0.6	0.7561		0.7506		0.7479	
	0.9	0.8712		0.8637		0.8602	
$\theta_{b,c}$	0.1	0.0761		0.0752		0.0748	
	0.3	0.3105		0.3071		0.3056	
	0.6	0.6074		0.6012		0.5984	
	0.9	0.7781		0.7696		0.7656	

n_x: Number of grid points in X-direction.
n_h, n_l and n_c: number of grid points in hot fluid, liquid film and air stream, respectively, in Y-direction

than 1 percent. Accordingly, the 61 × 136 grid was used in the subsequent computations. To check the adequacy of the numerical scheme employed for the present study further, results for the limiting case of laminar forced convection heat transfer between parallel plates were obtained. Excellent agreement was found between the present predictions and those of Heaton et al. (1964). Another limiting case is the combined heat and mass transfer in moist air stream flowing over an extremely thin liquid film. The predicted results agreed well with those of Lin et al. (1988). This lends support to the employment of the present numerical scheme.

Results and discussion

In the present study calculations are specifically carried out for the system with hot liquid water on the hot sides and moist air flowing over a falling liquid water film on the cold sides of the multichannel wet surface heat exchanger plates, a situation widely encountered in thermal systems. It should be emphasized herein that not all the values for the nondimensional parameters appearing in the study, that is, Re_h, $Re_{l,in}$, $Re_{c,in}$, Pr_h, Pr_l, Pr_c, Sc, μ_c/μ_l, k_c/k_l, k_h/k_l, ρ_c/ρ_l, $u_{c,in}/u_{l,in}$, L, $\delta_{l,in}/(b/2)$ and so on, can be arbitrarily assigned. In fact, some of them are interdependent under certain specific conditions.

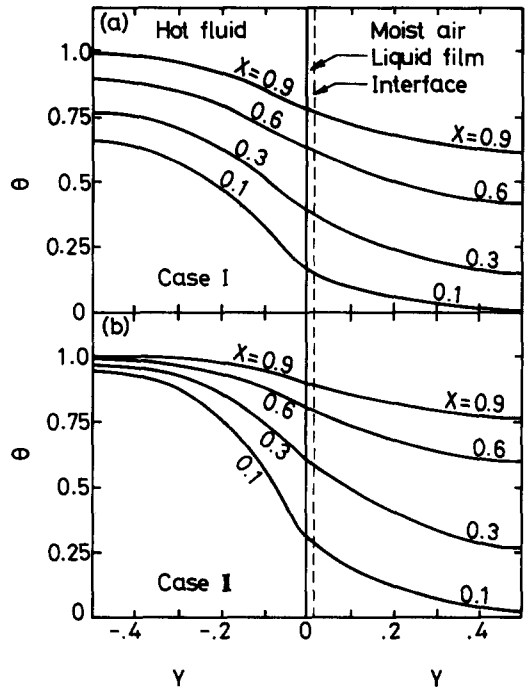

Figure 2 Developments of dimensionless temperature profiles for $Re_{c,in} = 1{,}000$, $Re_{l,in} = 200$, $\varphi_{in} = 0.5$, $T_{h,in} = 60°C$ and (a) $Re_h = 500$, (b) $Re_h = 1{,}500$

In light of practical situations, Re_h, $Re_{l,in}$, $Re_{c,in}$, L, $T_{h,in}$, $T_{l,in}$, $T_{c,in}$, b and ϕ_{in} are selected as the independent physical parameters. Then the other parameters can be evaluated. Furthermore, to be more concentrated on the effects of Re_h, $Re_{l,in}$, $Re_{c,in}$, $T_{h,in}$ and ϕ_{in} on the heat- and mass-transfer characteristics in the exchanger, the results are presented for a system with b fixed at 1 cm, $T_{c,in} = T_{L,in} = 30°C$ and $L = 200$. The values of the parameters for various cases to be studied are given in Table 2.

Shown in Figure 2 are the temperature profiles in the hot liquid water, liquid film and moist air flows for cases with $Re_{l,in} = 200$, $Re_{c,in} = 1{,}000$, $T_{h,in} = 60°C$, $T_{l,in} = T_{c,in} = 30°C$ and $\phi_{in} = 30$ percent at different Re numbers of the hot liquid flow. The results indicate that the temperatures of the hot fluid decrease monotonically in the respective downstream direction of the hot fluid. The energy rejected by the hot fluid heats up the liquid film and air stream, and thus their temperatures increase with X. A comparison of the corresponding curves in Figures 2a and b at the same X illustrates that a larger Re_h results in a smaller temperature drop of the hot fluid, but a higher temperature rise of the liquid film and air stream. The mass

Table 2 Values of parameters for various cases

Case	Re_h	$Re_{l,in}$	$Re_{c,in}$	$T_{h,in}$°C	ϕ_{in}	Pr_h	Pr_l	$u_{c,in}/u_{l,in}$	$\delta_{l,in}/(b/2)$
I	500	200	1,000	60	0.5	3.4	4.2	5.33	0.0423
II	1,500	200	1,000	60	0.5	3.1	4.0	5.33	0.0423
III	1,000	100	1,000	60	0.5	3.2	3.9	8.11	0.0336
IV	1,000	200	1,000	60	0.5	3.3	4.1	5.33	0.0423
V	1,000	200	1,000	50	0.5	3.8	4.5	5.33	0.0423
VI	1,000	500	1,000	60	0.5	3.4	4.2	2.78	0.0574
VII	1,000	200	2,000	60	0.5	3.4	4.1	10.22	0.0423
VIII	1,000	200	1,000	60	0.8	3.3	4.1	5.33	0.0423

$Pr_c = 0.71$, $S_c = 0.58$, $\mu_c/\mu_l = 0.031$, $k_c/k_l = 0.043$, $k_{h/kl} = 1.01$ and $\rho_c/\rho_l = 0.0011$.

fraction profiles of the water vapor in the moist air stream are plotted in Figure 3. It is observed that as the moist air goes downstream, the mass fraction of the water vapor in it gradually increases owing to the evaporation of liquid film into the air stream. In addition, the mass fraction of the water vapor at the interface increases in the flow direction, and more water vapor exists at the interface when Re_h is higher. These trends are similar to the interface temperature developments given in Figure 2 because thermodynamic equilibrium was assumed at the interface (Equation 12).

Knowing the evaporation rate of the falling liquid film is important in improving our understanding of the heat- and mass-transfer processes in the exchanger. Additionally, the consumption of the liquid water owing to the film vaporization is interested in the engineering applications. To meet these ends, a nondimensional evaporation rate of the liquid film is introduced.

$$Em = \int_0^x m''_{v,i} dx / \dot{m}_{l,in} \tag{30}$$

where $\dot{m}_{l,in} = (Re_{l,in}\mu_l)/4$ (Bird et al. 1960) is the liquid-film inlet mass-flow rate per unit channel depth. Em can be represented in dimensionless variables as

$$Em = \left(\frac{4L}{Re_{l,in}}\right)\left(\frac{\mu_c}{\mu_l}\right)\left(\frac{w_r - w_{in}}{Sc}\right)\int_0^X -\left(\frac{\partial W/\partial Y}{1-w}\right)_i dX \tag{31}$$

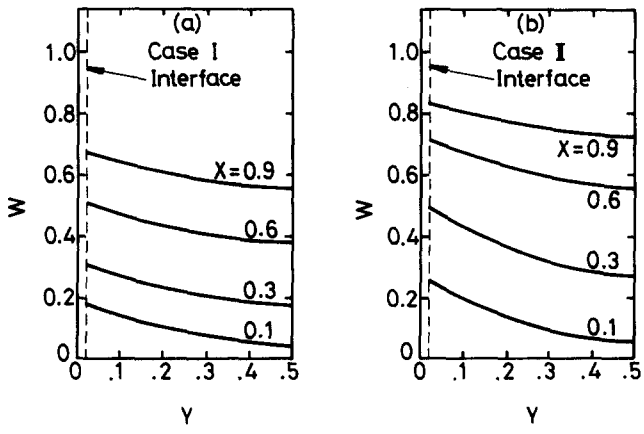

Figure 3 Developments of mass fraction profiles of water vapor in moist air stream for $Re_{c,in} = 1{,}000$, $Re_{l,in} = 200$, $\phi_{in} = 0.5$, $T_{h,in} = 60°C$ and (a) $Re_h = 500$, (b) $Re_h = 1{,}500$

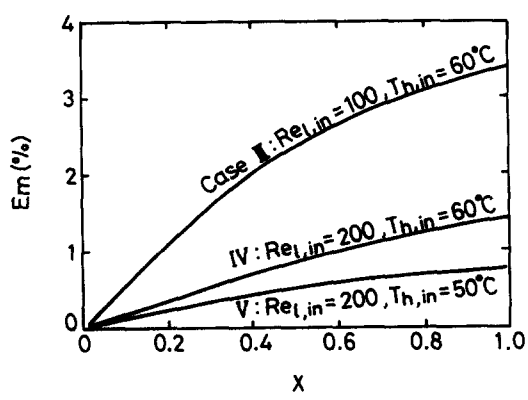

Figure 4 Distributions of the dimensionless film vaporization rate for $Re_h = Re_{c,in} = 1{,}000$ and $\phi_{in} = 0.5$

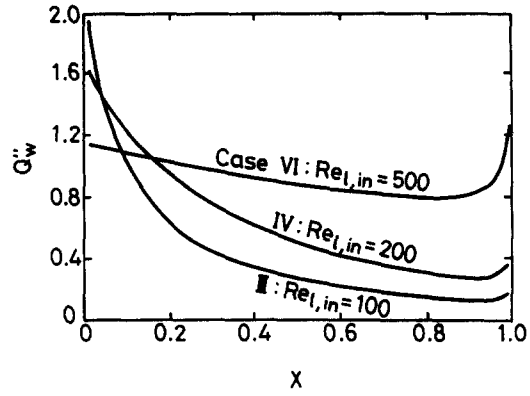

Figure 5 Dimensionless wall heat flux distributions for $Re_h = Re_{c,in} = 1{,}000$, $T_{h,in} = 60°C$ and $\phi_{in} = 0.5$

The effects of $Re_{l,in}$ and $T_{h,in}$, on the variations of Em are demonstrated in Figure 4. For the system with lower $Re_{l,in}$ or higher $T_{h,in}$ larger film vaporization is observed. This can be attributed to the fact that the temperature rise in the liquid film heated up by the hot fluid is higher for a system with a smaller $Re_{l,in}$ or higher $T_{h,in}$, which then causes a higher concentration of water vapor at interface. The results for Em in Figure 4 clearly show that the mass loss of liquid film because of evaporation is relatively small.

In practical applications the heat-transfer rate in the exchanger is of considerable interest. Shown in Figure 5 are the distributions of the dimensionless wall heat flux, $Q''_w = -(\partial\theta_h/\partial Y)_{Y=0}$. It is observed that Q''_w sharply increases with X in the respective inlet region of the hot fluid flow, which is directly caused by the entrance effects of the hot flow. Also noted in Figure 5 is that Q''_w is higher for a system with larger $Re_{l,in}$ in the middle region and at the end region near $x = 1$. However, the trend is reversed in the region near $X = 0$.

Physically, a portion of the energy rejected by the hot fluid goes to heat up the liquid film and the other portion of the energy transports across the film to cause the vaporization of liquid film and temperature rise of the air stream. To illustrate the effectiveness of latent heat transfer through film vaporization, the interface latent heat flux absorbed by the film vaporization $q''_e = m''_{v,i} h_{fg}$, interface sensible heat flux in the air side $q''_s = -k_c(\partial T_c/\partial y)_{y=\delta_l}$ and total interface heat flux $q''_i = q''_e + q''_s$ are contrasted with the energy rejected by the hot fluid to the film $q''_r = -k_h(\partial T_h/\partial y)_{y=0}$. Figures 6a–c present the distributions of q''_e/q''_r, q''_s/q''_r and q''_i/q''_r, for cases with various $Re_{l,in}$. First, by comparing the ordinate scales of Figures 6a and b, it is apparent that q''_e/q''_r is much larger than q''_s/q''_r. For a fixed $Re_{l,in}$, q''_e/q''_r is about 10 times larger than q''_s/q''_r. This indicates that the energy transfer across the film is mostly absorbed by the process of film vaporization. Also noted in Figure 6 is that a lower $R_{l,in}$ results in a higher q''_e/q''_r because of the higher temperature rise of the liquid film and, consequently, stronger film vaporization at the interface. Similar trends can be seen in the sensible heat transfer at interface (Figure 6b), which is simply due to the larger temperature difference between the interface and air stream for the case with lower $Re_{l,in}$. The distributions of the dimensionless total heat flux at interface q''_i/q''_r given in Figure 6c show that a substantial portion of the rejected heat transports across the liquid film at lower $Re_{l,in}$.

The influences of the Reynolds number $Re_{c,in}$ and inlet relative humidity in the moist air on the distributions of q''_e/q''_r, q''_s/q''_r and q''_i/q''_r are given in Figures 7a–c. It is observed in

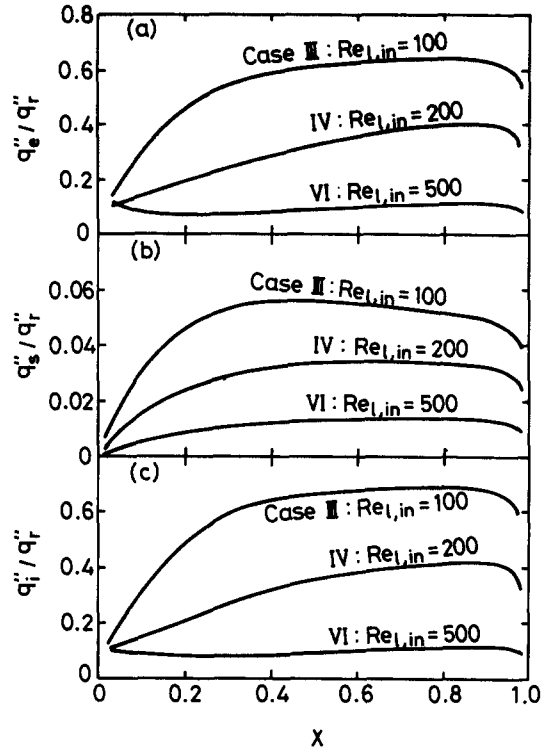

Figure 6 Dimensionless local heat flux distributions at film-air interface for $Re_h = Re_{c,in} = 1{,}000$, $T_{h,in} = 60°C$, $\phi_{in} = 0.5$; (a) latent heat, (b) sensible heat and (c) overall

Figures 7a and c that q_e''/q_r'' and q_i''/q_r'' are higher for the case with higher $Re_{c,in}$, because of stronger film vaporization at the interface associated with it. An inspection of Figure 7 shows that the influences of ϕ_{in} on the variations of q_e''/q_r'', q_s''/q_r'' and q_i''/q_r'' are insignificant.

As noted earlier, the latent heat transport in connection with the film vaporization at the interface plays an important role for the thermal performance of the wet surface heat exchanger. Attention is now turned to investigating the coefficients of the heat and mass transfer from the interface to the air stream. Equation 13 indicates that energy transported from the film-air interface into the air stream depends on two related factors: the interfacial temperature gradient on the air side, resulting in a sensible heat transfer, and the rate of mass transfer, resulting in latent heat transfer. The total heat transfer from the interface into the air stream can then be expressed as

$$q_i'' = q_s'' + q_e'' = -\left(k_c \frac{\partial T_c}{\partial y}\right)_i - \left(\frac{\rho_c D h_{fg}}{1 - w_i}\right) \cdot \left(\frac{\partial w}{\partial y}\right)_i \tag{32}$$

The local Nusselt number at the interface

$$Nu_i = \frac{h_t b}{k_c} = \frac{q_i'' b}{k_c (T_{l,i} - T_{c,b})} \tag{33}$$

can be written as

$$Nu_i = Nu_s + Nu_e \tag{34}$$

where Nu_s and Nu_e are, respectively, the local Nusselt numbers for sensible and latent heat transfer, and are evaluated by

$$Nu_s = \frac{b(-\partial T_c/\partial y)_i}{T_{l,i} - T_{c,b}} = -\frac{(\partial \theta_c/\partial Y)}{\theta_{l,i} - \theta_{c,b}} \tag{35}$$

$$Nu_e = \frac{\rho_c D h_{fg} b(-\partial w/\partial y)_i}{k_c (T_{l,i} - T_{c,b})(1 - w_i)} = -\frac{S}{(\theta_{l,i} - \theta_{c,b})(1 - w_i)} \left(\frac{\partial W}{\partial Y}\right)_i \tag{36}$$

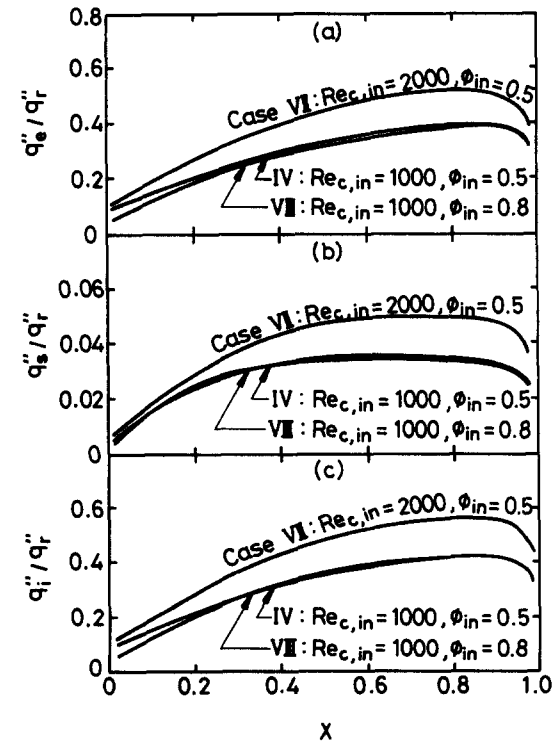

Figure 7 Dimensionless local heat flux distributions at film-air interface for $Re_h = 1{,}000$, $Re_{l,in} = 200$, $T_{h,in} = 60°C$; (a) latent heat, (b) sensible heat and (c) overall

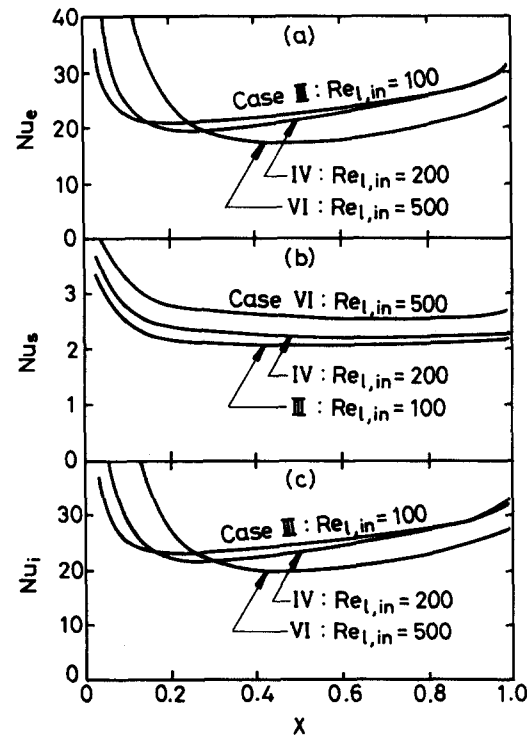

Figure 8 Distributions of local Nusselt numbers along the film-air interface for $Re_h = Re_{c,in} = 1{,}000$, $T_{h,in} = 60°C$, $\phi_{in} = 0.5$; (a) latent heat, (b) sensible heat and (c) overall

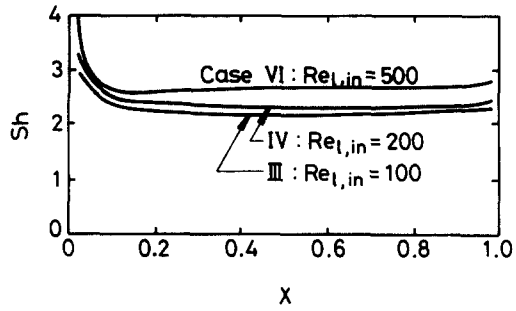

Figure 9 Distributions of local Sherwood number along the film-air interface for $Re_h = Re_{c,in} = 1{,}000$, $T_{h,in} = 60°C$ and $\phi_{in} = 0.5$

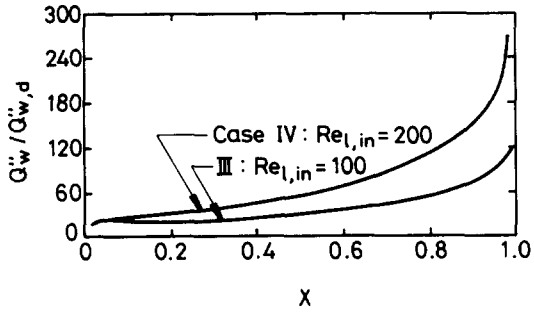

Figure 10 Distributions of $Q''_w/Q''_{w,d}$ for $Re_h = Re_{c,in} = 1{,}000$ $T_{h,in} = 60°C$ and $\phi_{in} = 0.5$

Here S signifies the relative importance of energy transport through species diffusion to that through thermal diffusion at the interface,

$$S = \frac{\rho_c D h_{fg}(w_r - w_{in})}{k_c(T_{h,in} - T_{c,in})} \tag{37}$$

Similarly, the local Sherwood number at the interface is defined as

$$\mathrm{Sh} = \frac{h_m b}{D} = -\frac{(\partial W/\partial Y)_i}{W_i - W_b} \tag{38}$$

To study the relative contributions of heat transfer through sensible and latent heat transfer at the interface, three kinds of Nusselt numbers are presented in Figure 8. As expected, the Nu_e is much higher than the Nu_s. In addition, Nu_e decreases with X and reaches a minimum value at a certain location. Beyond that it gradually increases. The results are the consequence of the continuous rise of the interface water-vapor concentration in the X-direction. Figure 9 presents the effects of $Re_{l,in}$ on the variations of Sh. Higher $Re_{l,in}$ results in higher Sh, which is similar to that for Nu_s.

Finally, the heat flux in the wet surface heat exchanger, Q''_w, is compared with that obtainable in the dry surface heat exchanger, $Q''_{w,d}$. The results in Figure 10 show that the heat-transfer rate is greatly enhanced when the wall surface is wetted by a thin liquid film.

Conclusion

A numerical analysis has been carried out to explore the detailed heat- and mass-transfer characteristics in a multi-channel wet surface heat exchanger. The effects of $Re_{h,in}$, $Re_{c,in}$, $Re_{l,in}$, $T_{h,in}$ and ϕ_{in} on the performance of the exchanger are examined in great detail. What follows is a brief summary of the major results:

1. The energy transported across the liquid film is mostly absorbed by the process of film vaporization, and only about 10 percent of the energy goes to heat up the moist air stream.
2. The Q''_w is much higher than the $Q''_{w,d}$, and $Q''_w/Q''_{w,d}$ drastically increases with X in the respective inlet region of the hot flow.
3. Results show that the mass loss of liquid film owing to evaporation is relatively small.

Acknowledgment

The financial support of this study by the engineering division of the National Science Council, Taiwan, ROC, through the contract NSC 81-0401-E-150-505 is greatly appreciated.

References

Bird, R. B., Stewart, W. E. and Lightfoot, E. N. 1960. *Transport Phenomena*. Wiley, New York, chap. 2

Eckert, E. R. G. and Drake, R. M., Jr. 1972. *Analysis of Heat and Mass Transfer*. McGraw-Hill, New York, chaps 20 and 22

El-Wakil, M. M. 1984. *Powerplant Technology*. McGraw-Hill, New York, chap.7

Guinn, G. R. and Novel, G. J. 1981. Operating performance of a water spray on an air type condensing unit. *ASHRAE Trans.*, **87**, 373–381

Heaton, H. S., Reynolds, W. C. and Kays, W. M. 1964. Heat transfer in annular passages: simultaneous development of velocity and temperature fields in laminar flow. *Int. J. Heat Mass Transfer*, **7**, 763–781

Holzhauer, R. 1979. Cooling system condensers. *Plant Engineering*, **32**, 74–81

Jang, W. J and Clark, D. W. 1975. Spray cooling of air-cooled compact heat exchangers. *Int. J. Heat Mass Transfer*, **118**, 311–317

Kafesgian, R., Plank, C. A. and Gerhard, E. R. 1961. Liquid flow and gas phase mass transfer in wetted-walls towers. *AICHE J.*, 7, 463–466

Kettleborough, C. F. and Hsieh, C. S. 1983. The thermal performance of the wet surface plastic plate heat exchanger used as an indirect evaporative cooler. *ASME J. Heat Transfer*, **105**, 366–373

Leidenfrost, W. and Korenic, B. 1979. Analysis of evaporative cooling and enhancement of condenser efficiency and of coefficient of performance. *Wärme-und stoffübertragung*, **12**, 5–23

Lin, T. F., Chang, C. J. and Yan, W. M. 1988. Analysis of combined buoyancy effects of thermal and mass diffusion on laminar forced convection heat transfer in vertical tube. *ASME J. Heat Transfer*, **110**, 337–344

Maclaine-Cross, I. L. and Banks, P. J. 1972. Coupled heat and mass transfer in regenerators: prediction using an analogy with heat transfer. *Int. J. Heat Mass Transfer*, **15**, 1225–1242

Maclaine-Cross, I. L. and Banks, P. J. 1981. A general theory of wet surface heat exchangers and its application to regenerative evaporative cooling. *ASME J. Heat Transfer*, **103**, 579–585

Mizushima, T., Ito, R. and Miyashita, H. 1967. Experimental study of an evaporative cooler. *Int. Chem. Eng.*, **7**, 727–732

Perez-Blanco, H. and Bird, W. A. 1984. Study of heat and mass transfer in a vertical-tube evaporative cooler. *ASME J. Heat Transfer*, **106**, 210–215

Pescod, D. 1979. A heat exchanger for energy saving in an air conditioning plant. *ASHRAE Trans.*, **85**, 238–252

Shembharkar, T. R. and Pai, B. R. 1986. Prediction of film cooling with a liquid coolant. *Int. J. Heat Mass Transfer*, **29**, 899–908

Stücheli, A. and Özisik, M. N. 1976. Hydrodynamic entrance length of laminar falling films. *Chem. Eng. Sci.*, **31**, 369–372

Tsay, Y. L., Lin, T. F. and Yan, W. M. 1990. Cooling of a falling liquid film through interfacial heat and mass transfer. *Int. J. Multiphase Flow*, **16**, 853–865

Wassel, A. T. and Mills, A. F. 1987. Design methodology for a counter-current falling film evaporative condenser. *ASME J. Heat Transfer*, **109**, 784–787